# *Ex vivo* and *in vivo* second-harmonic-generation imaging of dermal collagen fiber in skin: comparison of imaging characteristics between mode-locked Cr:forsterite and Ti:sapphire lasers

Takeshi Yasui,* Yu Takahashi, Masahiro Ito, Shuichiro Fukushima, and Tsutomu Araki

Graduate School of Engineering Science, Osaka University, 1-3 Machikaneyama-cho, Toyonaka, Osaka 560-8531, Japan

*Corresponding author: t-yasui@me.es.osaka-u.ac.jp

Received 2 September 2008; revised 22 December 2008; accepted 26 December 2008; posted 5 January 2009 (Doc. ID 100978); published 26 January 2009

Second-harmonic-generation (SHG) microscopy is an interesting new tool for observing dermal collagen fiber in skin. However, conventional SHG microscopy using a mode-locked Ti:sapphire laser suffers from low penetration depth and a slow image acquisition rate caused by scattering and absorption in tissue, making it difficult to use for *in vivo* applications on human skin. We develop an SHG microscope equipped with a mode-locked Cr:forsterite laser with a long wavelength and compare its imaging characteristics with that of a Ti:sapphire-laser-based SHG microscope for the measurement of dermal collagen fiber in animal and human skins. The results indicate the suitability of the Cr:forsterite laser-based SHG microscope for *in vivo* imaging of human skin. © 2009 Optical Society of America

*OCIS codes:* 170.1870, 170.3880, 170.6960, 180.4315, 190.4160.

## 1. Introduction

Dermal collagen fiber plays an important role in determining morphological and mechanical properties of skin as a structural protein. Therefore, there is a great need for an appropriate monitoring tool that can reveal the three-dimensional (3D) structure of dermal collagen fibers *in vivo*. Recently, second-harmonic-generation (SHG) microscopy with a near-infrared femtosecond pulse laser has received interest as an optical probe method to investigate collagen fiber in biological tissues due to the fact that biological SHG light is specifically generated by collagen molecules [1,2]. This SHG light also provides unique imaging modality: high contrast, high spatial resolution, optical 3D sectioning, noninvasive, and deep penetration. By using endogenous SHG as a contrast mechanism, this microscopy enables visualization of the structures of collagen fiber in tissues without additional staining and hence avoids phototoxicity and photobleaching. By taking advantage of these characteristics, SHG microscopy has been applied to visualize detailed structures of dermal collagen fiber in skin [3,4]. In addition, combining this technique with polarization methods, namely, polarization-resolved SHG microscopy, can give additional insights with regard to the orientation of collagen fiber in tissues and has been used to quantify the collagen fiber orientation in the dermis [5–7].

In most previous studies, a mode-locked Ti:sapphire (Ti:S) laser with a center wavelength around 800 nm was used as the light source to generate SHG light around 400 nm [2–7]. However, scattering and absorption of the skin at these wavelengths often limits *in vivo* monitoring of dermal collagen fiber in a reflection configuration. Multiple

0003-6935/09/100D88-08$15.00/0

scattering events greatly reduce the number of ballistic photons of the incident laser light, which is the dominant source of nonlinear excitation in deep focusing nonlinear microscopy [8], although the scattering does not significantly degrade the profile of the point spread function at the focal spot [8,9]. In the return path, 400 nm SHG light is largely attenuated by severe multiple scattering and absorption. These effects lead to an insufficient penetration depth for *in vivo* monitoring of the dermal collagen fiber across the stratum corneum and epidermis layers in a reflection setup. For polarization-resolved SHG microscopy, multiple scattering events further depolarize the detected SHG light, resulting in decreased sensitivity to collagen fiber orientation in deep regions of tissue [7]. Another problem with *in vivo* applications for human skin is the risk of biological photodamage in the vicinity of the focal spot caused by nonlinear absorption and/or ionization of the incident laser light [10,11]. The problems of conventional Ti:S laser-based SHG microscopy can be addressed by the use of an ultrashort pulse laser with a longer wavelength to suppress multiple scattering and absorption in tissue. In a promising alternative laser source for SHG microscopy, the Ti:S laser is replaced with a mode-locked Cr:forsterite (Cr:F) laser centered around 1250 nm, which takes advantage of the fact that absorption and scattering in tissue is minimum near a wavelength of 1300 nm [12,13]. Recently, combined SHG and third-harmonic-generation microscopy using a Cr:F laser was effectively applied to *in vivo* developmental biology of zebrafish embryos [14], the optical biopsy of a hamster oral cavity [15], fixed human skin [16], and teeth [17]. Few studies have directly compared the SHG imaging performance of Ti:S and Cr:F lasers, although plant tissue cell damage under irradiation of tightly focused beams has been compared [18]. Here we report the construction of two equivalent reflection-mode SHG microscopes equipped, respectively, with a Ti:S laser and a Cr:F laser. We compare their imaging characteristics by *ex vivo* and *in vivo* measurements of dermal collagen fiber in animal and human skins.

## 2. Experimental Setup

As a light source for the SHG microscopes, we employed an 800 nm Ti:S laser (Spectra Physics, MaiTai; 100 fs pulse duration, 800 mW average power, 80 MHz repetition rate) and a 1250 nm Cr:F laser (Avesta Project, Moscow Region, Russian Federation, CrF-65P; 135 fs pulse duration, 200 mW average power, 73 MHz repetition rate). The experimental setup for the SHG microscope is illustrated in Fig. 1. For rapid acquisition of SHG images, the laser beam is scanned in two dimensions by a pair of galvano mirrors (GM). After passing through relay lenses (RL1 and RL2), the laser beam is focused onto the sample with an objective lens (OL; Nikon Instruments, Melville, New York, CFI Plan 50 × H, 50 magnification, 0.9 numerical aperture, 350 $\mu$m working distance, oil immersion). The immersion oil for the OL decreases the reflection loss and spherical aberration caused by mismatching the refractive index at the sample surface. The OL can be moved along the optical axis by a piezoelectric transducer (PZT, stroke length of 350 $\mu$m). Combining the GM and the PZT enables optical 3D sectioning images of SHG light to be taken. The average power of both lasers on the sample was set to 40 mW. Although the dwell time of the high power can be reduced by adjusting the excitation power with depth, we kept the laser power at this power level for ease of comparison. Whereas the SHG light induced in the sample propagates mainly in the same direction as the incident laser light, a portion of the generated SHG light is backscattered into the sample. This backscattered SHG light, which is the main signal source of SHG imaging in the reflection setup, is collected via the OL. The SHG light is descanned by the GM and separated from the laser light by a harmonic separator (HS, reflected wavelength of 400 nm for Ti:S SHG light or 625 nm for Cr:F SHG light) and an infrared-cut filter (F). The SHG light is detected by a combined photon-counting photomultiplier tube (PMT) and pulse counter. To suppress the wavelength dependence of the PMT sensitivity, we used a different PMT with the same sensitivity at wavelengths of 400 and 625 nm for each SHG microscope (Hamamatsu Photonics K.K. 7155-20 with a count sensitivity of $2.7 \times 10^5\ s^{-1}\ pW^{-1}$ for Ti:S SHG light and H8259-01 for Cr:F SHG light with a count sensitivity of $2.3 \times 10^5\ s^{-1}\ pW^{-1}$). Since the PMT for the Ti:S SHG microscope has an internal prescaler that scales the signal down by a factor of 4, we multiply the measured photon count by four. Since the field of view of the microscope can be changed by scanning the angle of the GM, we adjusted the field of view size to fit observed structures of dermal collagen fibers within the range of the image.

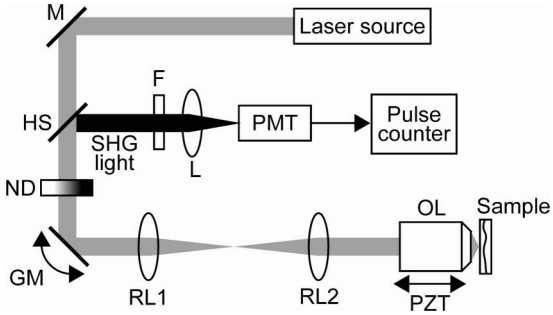

Fig. 1. Experimental setup: M, mirror; HS, harmonic separator; ND, neutral density filter; GM, galvano mirrors; RL1 and RL2, relay lenses; OL, oil-immersion objective lens; PZT, piezoelectric transducer; F, infrared-cut filter; PMT, photon-counting photomultiplier tube; L, lens.

In this way, we designed a descanned collection system for SHG light; many nonlinear microscopes are based on a nondescanned collection system for efficient collection of scattered SHG light. Our interest is in the *in vivo* application of polarization-resolved SHG microscopy for examining

skin, and since multiple scattering depolarizes the SHG light and hence decreases the sensitivity to collagen fiber orientation [7], it is important to reject unnecessary multiple-scattered SHG light efficiently when probing the deep regions of skin with polarization-resolved SHG microscopy. To reject multiple-scattered SHG light, a descanned collection system is more suitable than a nondescanned system because the former detects the ballistically backscattered SHG light with little depolarization rather than multiple-scattered SHG light.

## 3. Results

### A. *Ex Vivo* Observation of Animal Skin

We first took *ex vivo* SHG images of a block sample excised from porcine skin, scanning the observation plane parallel to the skin surface along the depth direction, namely depth-resolved SHG imaging. We used the back skin of a Yucatan micropig purchased from Charles Rivers Laboratories (Wilmington, Massachusetts) as a sample. The excised skin tissue was embedded in optical cutting temperature (OCT) compound (Sakura Finetek, Tokyo, Japan) and snap frozen in liquid nitrogen. A frozen block of the skin tissue was sliced to 5 mm thickness parallel to the skin surface. Then the dermal collagen fiber was measured across the stratum corneum and epidermis layers by the two SHG microscopes. Figures 2(a) and 2(b) show two series of depth-resolved SHG images measured with the Ti:S SHG and Cr:F SHG microscopes with the probing depth from the skin surface varied in 50 $\mu$m intervals. To compare two SHG images with different photon counts, we scaled them to grayscale images with 256 gradations for each image. Note however that the imaging area on a sample for the Ti:S SHG microscope is not consistent with that for the Cr:F SHG microscope. Although it might be better to perform the image comparison with the same area on a sample, it is difficult for the two SHG microscopes to image exactly the same area on a sample because the two laser sources used in this study were set in different experimental rooms and we had to construct two independent SHG microscopes. Consecutive depth-resolved SHG images at depth intervals of 10 $\mu$m are also shown as a movie (Media 1) of Fig. 2. The area of each image is 400 $\mu$m by 400 $\mu$m, composed of 256 pixels by 256 pixels. The image acquisition rate is 10 s/image. In the Ti:S SHG images, the SHG signal first appears at a depth of 80 $\mu$m below the skin surface [see the movie (Media 1) in Fig. 2], which indicates that the analytical spot enters the collagen-rich dermis layer from the no-collagen epidermis layer. The distribution of the collagen fiber in the papillary dermis was imaged. However, the Ti:S SHG image rapidly became out of focus when the probing depth exceeded 110 $\mu$m, and the SHG light almost disappeared beyond a depth of 200 $\mu$m. Because of this, the measurable depth of the Ti:S SHG microscope was limited to a shallow

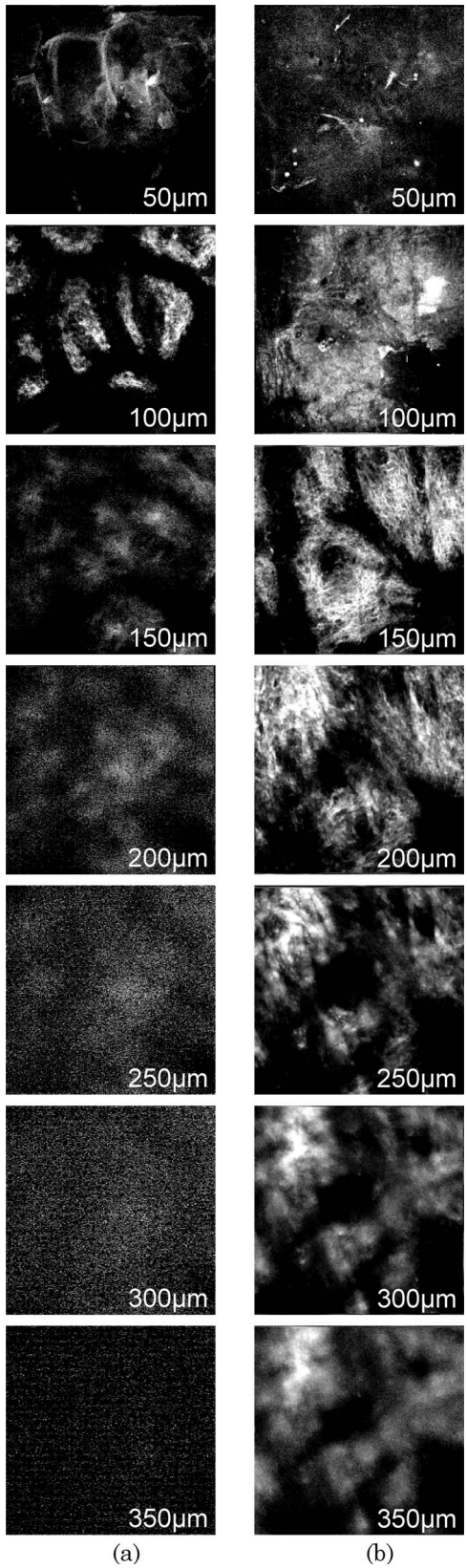


Fig. 2. Depth-resolved SHG imaging of dermal collagen fiber in porcine skin measured with (a) Ti:S SHG microscope and (b) Cr:F SHG microscope at 50 $\mu$m intervals. The image size is 400 $\mu$m by 400 $\mu$m and the image acquisition rate is 10 s/image. The movie (Media 1) shows consecutive change of their depth-resolved SHG images at 10 $\mu$m intervals.

region of the dermis. The Cr:F SHG microscope allowed depth-resolved SHG imaging to a deeper region of the dermis. As for the Ti:S SHG, the Cr:F SHG signal from dermal collagen fiber starts to appear after a depth of 80 $\mu$m. A structural change in the dermal collagen fiber is clearly visualized, depending on the probing depth. Within a depth region from 90 to 110 $\mu$m, the fine collagen fiber is distributed uniformly while the capillary vessels and pores without collagen content appear as black spots, which are specific characteristics in the papillary dermis layer. Even beyond a 120 $\mu$m depth, at which point the Ti:S SHG microscope rapidly loses its spatial resolution accompanied by a decrease of signal-to-noise ratio, the Cr:F SHG microscope maintains a sufficient spatial resolution to image the collagen fiber in the reticular dermis layer, in which the dermal collagen fibers gradually become thick. The Cr:F SHG image starts to become out of focus and lose sharpness beyond a 250 $\mu$m depth, however, a SHG signal was detected even at a depth of 350 $\mu$m. Since the maximum probing depth of the present Cr:F SHG microscope is limited by the working distance of the OL and the PZT ($=350\,\mu$m), using a longer working distance will increase the penetration depth beyond 350 $\mu$m. In this way, a comparison of depth-resolved SHG images of porcine skin for the Ti:S SHG and Cr:F SHG microscopes indicates that the latter is superior to the former with respect to high penetration power, which is important for *in vivo* observation of dermal collagen fiber in human skin. In usual nonlinear microscopes, spherical aberration of the OL, caused by mismatching of the refractive index at the sample surface, distorts and broadens the point spread function profile at deep probing regions, resulting in an out-of-focus SHG image and/or a weak SHG signal at the deep regions of the skin [19]. Refractive indices of the skin tissues are 1.51 for stratum corneum, 1.34 for epidermis, and 1.41 for dermis [20]. Since the refractive index of the immersion oil used here is 1.515, the mismatch of the refractive index at the skin surface (oil–corneum interface) is 0.005. Furthermore, when focusing the laser light on the layered tissue structure of the skin by the OL, additional mismatch of the refractive index occurs at interfaces between different tissue layers: 0.17 for the corneum–epidermis interface and 0.105 for the epidermis–dermis layer. These mismatches result in spherical aberration. Multiple scattering in tissues attenuates both the incident laser light and the detected SHG light. In Fig. 2, the resolution of the Ti:S SHG images is comparable to that of the Cr:F SHG images for depths between 50 and 100 $\mu$m. However, the resolution of the former degrades rapidly beyond a depth of 100 $\mu$m. Since the wavelength dependence of the spherical aberration is considered to be small, the difference in the image degradation between the two SHG microscopes is mainly due to the wavelength dependence of multiple scattering. The SHG image degradation at deep regions of the skin can be simply suppressed by introducing a confocal pinhole in the descanned collection system, at the expense of the SHG signal. Furthermore, both the SHG efficiency and the image quality improve if the spherical aberration of the OL is well compensated by adaptive optics [21,22].

We next evaluated the imaging characteristics of both SHG microscopes for rapid measurement. The probing depth was fixed at 140 $\mu$m from the surface of the porcine skin, so that SHG images of the dermal collagen fiber were measured. Figures 3(a) and 3(b) show Ti:S SHG images at an acquisition time of 10 and 1 s, respectively. The area of each image is 200 $\mu$m by 200 $\mu$m, composed of 256 pixels by 256 pixels. A sufficient photon count was not obtained for either 1 or 10 s acquisition times. Therefore, it is difficult to measure a fine SHG image rapidly at this probing depth with the Ti:S SHG microscope. Cr:F SHG images for measurement times of 10 and 1 s are shown in Figs. 3(c) and 3(d). Comparing the two Cr:F SHG images shows no degradation of image quality for a shorter image acquisition time because the photon count of the 10 s SHG image greatly exceeds the 256 gradations of the grayscale image. A clear SHG image of the dermal collagen fiber was obtained at the measurement time of 1 s. Furthermore, the photon counting rate achieved by the Cr:F SHG was several times higher than that achieved by the Ti:S SHG, despite the fact that the pulse width of the Cr:F laser is longer than that of the Ti:S laser. These results demonstrate the potential of Cr:F SHG imaging for *in vivo* applications on human skin from the viewpoint of a fast imaging rate.

The concentration gradient of the dermal collagen fiber along the depth direction is another important factor determining the morphological properties of

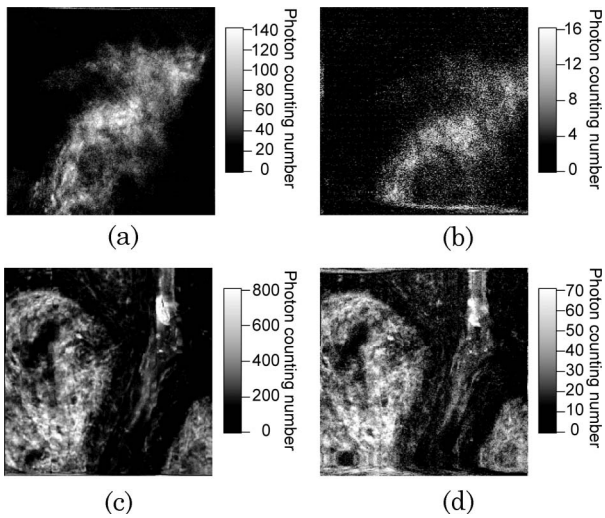


Fig. 3. Rapid SHG imaging of dermal collagen fiber in porcine skin. Ti:S SHG images at acquisition times of (a) 10 s and (b) 1 s, and Cr:F SHG images at acquisition times of (c) 10 s and (d) 1 s. The image size is 200 $\mu$m by 200 $\mu$m. The probing depth is fixed at 140 $\mu$m from the surface of the skin.

skin. Cross-sectional imaging by SHG light can reveal the gradient of the collagen fiber concentration in skin. Recently, SHG OCT was achieved by combining SHG imaging and OCT techniques and applied for cross-sectional imaging of collagen fiber in tissues [23,24]. However, the time required to acquire one cross-sectional image is longer than 5 min, even though coherent detection is used to enhance the weak SHG light. SHG microscopy also enables cross-sectional SHG imaging, namely, SHG tomography, by B-mode scanning by a tightly focused beam spot [25]. The high penetration capability and SHG efficiency achieved by the Cr:F SHG microscope are attractive for such SHG tomography of dermal collagen fiber. We performed SHG tomography of the back skin of a hairless mouse using the Cr:F SHG microscope. The preparation protocol of the skin specimen is similar to that used for the porcine skin. Figure 4(a) shows a series of cross-sectional SHG images measured with the Cr:F SHG microscope with the position of the B-mode scan laterally varied at 45 $\mu$m intervals. Confocal cross-sectional images of the reflectance fundamental light were also measured simultaneously, as shown in Fig. 4(b). Consecutive cross-sectional SHG and confocal reflectance images at 7.5 $\mu$m lateral intervals are also illustrated as a movie (Media 2) of Fig. 4. The area of each image is 300 $\mu$m width by 300 $\mu$m depth, composed of 256 pixels by 256 pixels. The imaging rate of the SHG tomography was 10 s/image, which is much smaller than that achieved by SHG OCT despite the fact that the image quality of our SHG tomography is comparable to that of SHG OCT. This is because photon counting detection was applied for the weak SHG light in addition to the high penetration power and SHG efficiency for the Cr:F laser. A comparison of the SHG images and confocal reflectance images reveals a line-shaped signal along the epidermis surface in the SHG images. Since the epidermis does not contain collagen fiber, we consider that this signal is due to third-harmonic-generation light caused by local optical inhomogeneities at the surface [16]. While no SHG area was observed underneath the skin surface, indicating that the epidermis layer does not contain collagen fiber, a strong SHG signal appeared in the dermis layer. Although it is difficult to evaluate a detailed cross section of the dermal collagen fiber due to insufficient depth resolution, the epidermal–dermal junctions, epidermal prolongations, and pores were resolved. In addition, the concentration gradient of the dermal collagen fiber in the skin could be estimated from the cross-sectional SHG image, although we have to consider the decrease of the SHG signal depending on the probing depth, caused by multiple scattering and absorption in tissue. The effect of SHG signal attenuation depending on depth is compensated by ratio imaging of SHG light to confocal reflectance light.

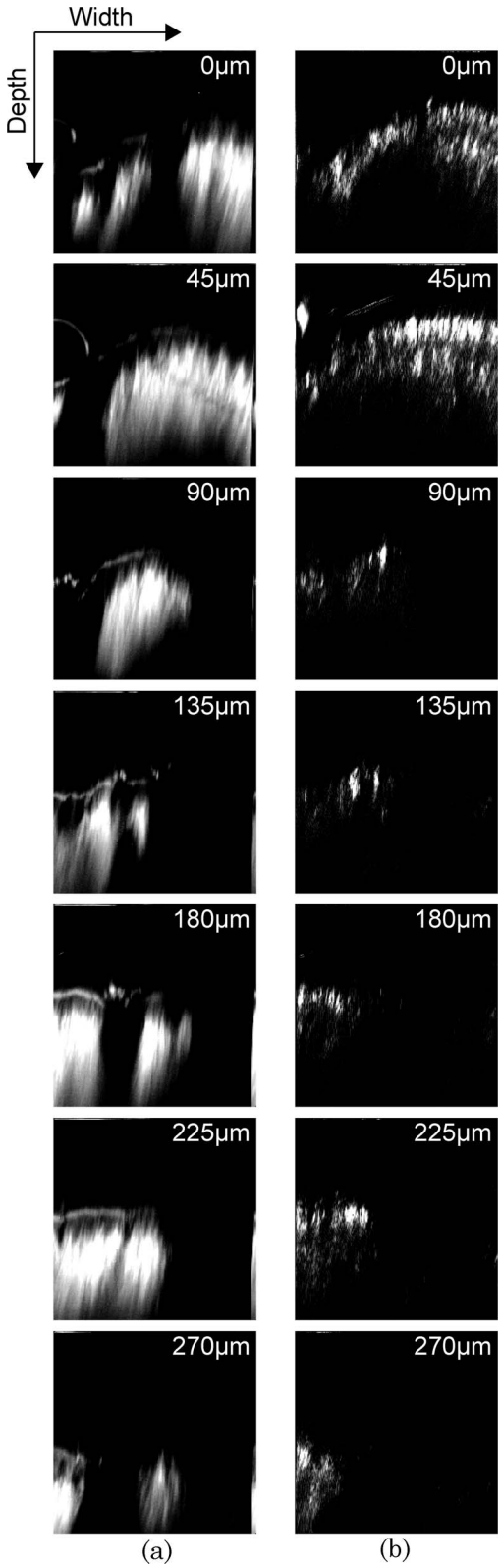


Fig. 4. Cross-sectional images of dermal collagen fiber in hairless mouse skin measured at lateral intervals of 45 $\mu$m: (a) Cr:F SHG images and (b) confocal reflectance image. The image size is 300 $\mu$m width by 300 $\mu$m depth, and the image acquisition rate is 10 s/image. The movie (Media 2) shows a consecutive change of their cross-sectional images at 7.5 $\mu$m lateral intervals.

### B. *In Vivo* Observation of Human Skin

When we apply SHG imaging to *in vivo* measurements of human skin, the risk of biological photodamage caused by nonlinear absorption and/or ionization in the vicinity of the focal spot must be considered. Although fluorescent antibody experiments have found that DNA damage of the epidermis caused by a 60 mW Ti:S laser irradiation is comparable to that caused by slight sunburn by 0.6-MED UV irradiation [26], such photodamage should not be ignored [10,11]. On the other hand, microspectroscopic comparison of the two lasers shows that the use of a Cr:F laser greatly reduces the cell damage to plant tissues [18]. Furthermore, little damage was observed on zebrafish embryos [14], hamster oral mucosa [15], and even human skin [27] by long-term irradiation by a tightly focused Cr:F laser beam. Based on these previous studies on biological photodamage and our comparisons of the imaging characteristics of the two lasers, we can conclude that the Cr:F SHG microscope is the best choice for *in vivo* observations of dermal collagen fiber in human skin.

An interesting application for *in vivo* observations of dermal collagen fiber is the assessment of cutaneous photoaging, which is necessary in fields such as anti-aging dermatology and skin cosmetic development. Biochemical, histochemical, and immunohistochemical experiments show that cutaneous photoaging is closely related to the amount and structure of dermal collagen fiber in the skin [28], and hence *in vivo* monitoring of dermal collagen fiber with the Cr:F SHG microscope may contribute greatly to the assessment of cutaneous photoaging. As a preliminary experiment for *in vivo* assessment of cutaneous photoaging, we here demonstrate *in vivo* depth-resolved SHG imaging of dermal collagen fiber of the forearm skin of a slightly sunburned 57-year-old male and a well sunburned 37-year-old male by use of the Cr:F SHG microscope. The inside and outside of the forearm skin are selected as *in vivo* measurement points to investigate the difference in dermal collagen fiber with and without cutaneous photoaging. Figures 5(a) and 5(b) show a series of depth-resolved SHG images of the inside and outside of the slightly sunburned forearm (57-year-old male) when the probing depth is varied at 50 $\mu$m intervals from the skin surface. Consecutive depth-resolved SHG images at 10 $\mu$m depth intervals are also illustrated as movies (Media 3) in Fig. 5. The area of each image is 600 $\mu$m by 600 $\mu$m with 256 pixels by 256 pixels. The image acquisition rate is 2 s/image. A detailed change in the collagen fiber distribution along the depth was visualized with high contrast images, although the movie (Media 3) of Fig. 5 exhibits fluctuations due to insufficient fastening of the forearm. On the inside of the forearm skin, the SHG images start to appear from a shallow skin depth and show that the fine collagen fiber of the papillary dermis layer is populated at shallow regions while the thick collagen fiber of the reticular dermis layer is observed at deep regions. The images

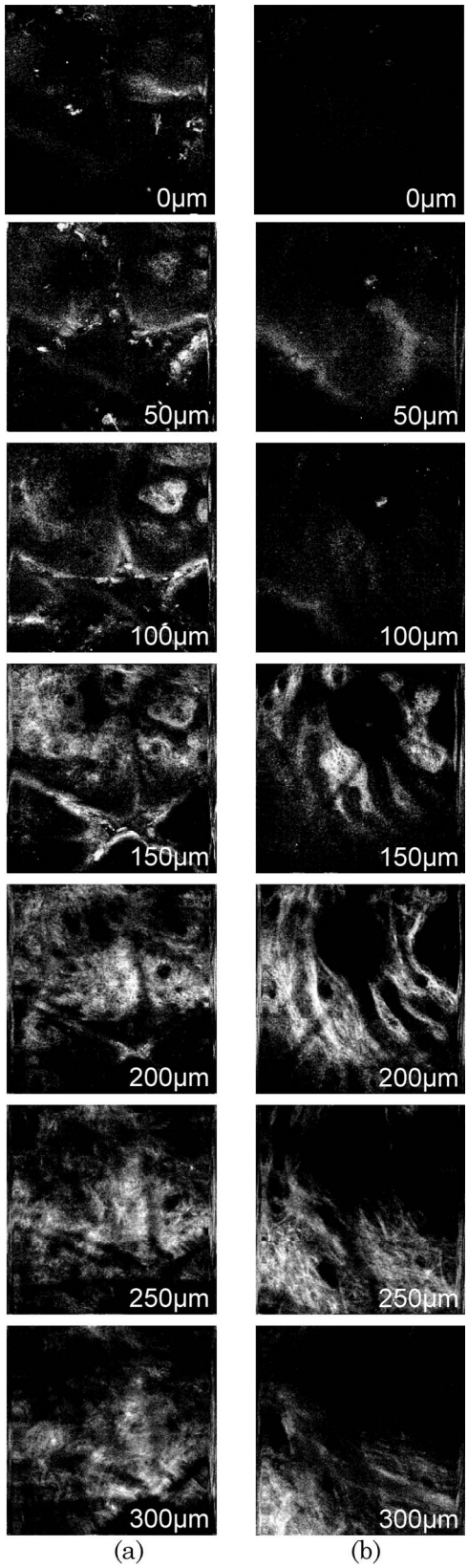


Fig. 5. *In vivo* depth-resolved Cr:F SHG imaging of forearm skin of a slightly sunburned 57-year-old male measured at 50 $\mu$m intervals (a) inside and (b) outside the forearm skin. The image size is 600 $\mu$m by 600 $\mu$m, and the image acquisition rate is 2 s/image. The movie (Media 3) shows consecutive change of their depth-resolved SHG images at 10 $\mu$m intervals.

also visualize pores, capillaries, and skin groove. On the outside of the forearm skin, the depth at which the SHG signal starts to appear is slightly deeper than for the inside forearm skin, indicating some small thickening of the epidermis caused by slight photoaging. Also, the characteristics of the dermal collagen fiber on the inside forearm skin shown in Fig. 5(a), namely, fine collagen fiber at shallow regions and thick collagen fiber at deep regions, were reproduced on the outside of the forearm skin. That is, there are no appreciable differences in the dermal collagen fiber between the inside and the outside of the slightly sunburned forearm. We next performed *in vivo* depth-resolved SHG imaging of the dermal collagen fiber on the inside and outside skin of the well sunburned forearm (37-year-old male), as shown in Figs. 6(a) and 6(b) and the corresponding movie (Media 4) (600 $\mu$m by 600 $\mu$m image size with 256 pixels by 256 pixels, image acquisition rate of 2s/image, and depth interval of 50 $\mu$m for the figure and 10 $\mu$m for the movie). On the inside of the forearm skin, the SHG images of the well sunburned forearm were similar to those of the slightly sunburned forearm [see Fig. 5(a)], indicating little influence of cutaneous photoaging on the inside of the forearm skin. Conversely, on the outside of the forearm skin, the depth at which the SHG signal starts to appear on the well sunburned forearm is deeper than that on the slightly sunburned forearm, indicating greater thickening of the epidermis and/or loss of dermal collagen fiber caused by advanced photoaging. Furthermore, the collagen fiber structure varies more gradually along the depth direction than for the outside skin of the slightly sunburned forearm. These results reflect the difference in dermal collagen fiber between photoaged skin and nonphotoaged skin. For a more detailed evaluation of cutaneous photoaging, a combination of SHG imaging and two-photon autofluorescence imaging [29,30] or polarization-resolved SHG microscopy for measuring collagen fiber orientation [31,32] will be useful.

## 4. Conclusions

We developed two equivalent reflection-mode SHG microscopes equipped with mode-locked Cr:F and Ti:S lasers for *ex vivo* and *in vivo* imaging of dermal collagen fiber in skin and compared their SHG imaging characteristics. For skin penetration capability, the Cr:F SHG microscope achieved a potential for penetration to a depth of over 350 $\mu$m, twice as deep as achieved by the Ti:S SHG microscope. Furthermore, comparison of the image acquisition rate between the two SHG microscopes indicated the suitability of the Cr:F SHG microscope. We performed *in vivo* depth-resolved SHG imaging of human forearm skin with and without sunburn using the Cr:F SHG microscope. This imaging clarified the difference in the dermal collagen fiber between photoaged skin and nonphotoaged skin. The results of this study show that Cr:F SHG microscopy has the

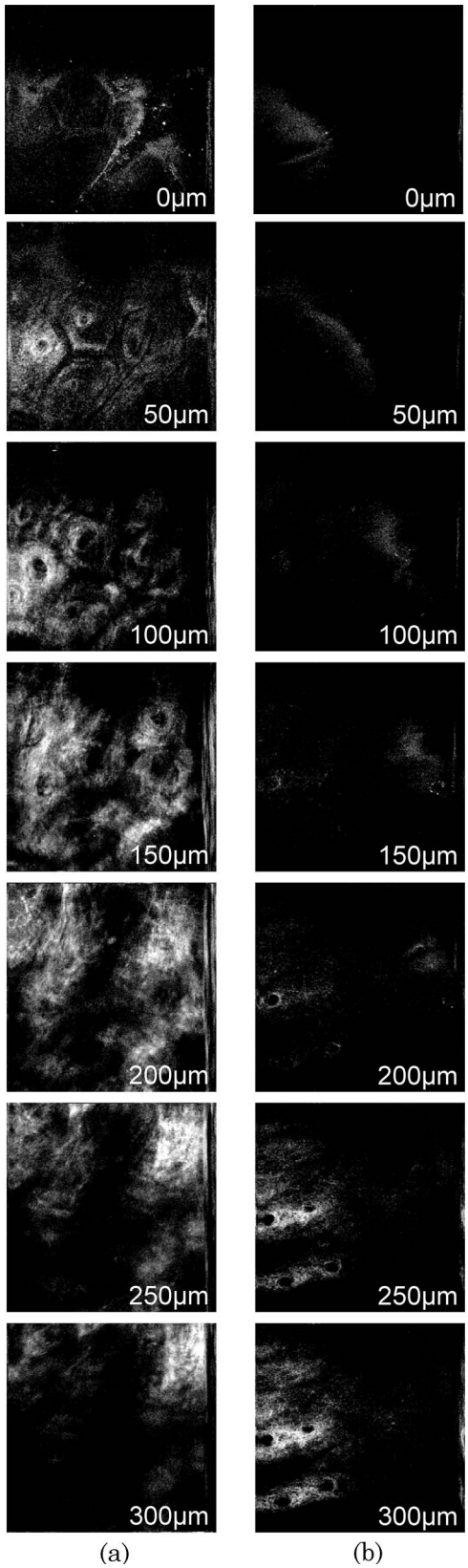


Fig. 6. *In vivo* depth-resolved Cr:F SHG imaging of forearm skin of a well sunburned 37-year-old male measured at 50 $\mu$m intervals (a) inside and (b) outside the forearm skin. The image size is 600 $\mu$m by 600 $\mu$m, and the image acquisition rate is 2 s/image. The movie (Media 4) shows consecutive change of their depth-resolved SHG images at 10 $\mu$m intervals.

potential to become a powerful tool for *in vivo* clinical applications on human skin.

This work was supported by Grants-in-Aid for Scientific Research Nos. 19650117 and 20240044 from the Ministry of Education, Culture, Sports, Science, and Technology of Japan. We also thank the Cosmetology Research Foundation, Japan, for financial support.

### References

1. S. Roth and I. Freund, "Optical second-harmonic scattering in rat-tail tendon," Biopolymers **20**, 1271–1290 (1981).
2. G. Cox, E. Kable, A. Jones, I. Fraser, F. Manconi, and M. D. Gorrell, "3-dimensional imaging of collagen using second harmonic generation," J. Structural Biol. **141**, 53–62 (2003).
3. K. König and I. Riemann, "High-resolution multiphoton tomography of human skin with subcellular spatial resolution and picosecond time resolution," J. Biomed. Opt. **8**, 432–439 (2003).
4. J. A. Palero, H. S. de Bruijn, A. van der Ploeg-van den Heuvel, H. J. C. M. Sterenborg, and H. C. Gerritsen, "In vivo nonlinear spectral imaging in mouse skin," Opt. Express **14**, 4395–4402 (2006).
5. T. Yasui, Y. Tohno, and T. Araki, "Determination of collagen fiber orientation in human tissue by polarization measurement of molecular second-harmonic-generation light," Appl. Opt. **43**, 2861–2867 (2004).
6. T. Yasui, Y. Tohno, and T. Araki, "Characterization of collagen orientation in human dermis by two-dimensional second-harmonic-generation polarimetry," J. Biomed. Opt. **9**, 259–264 (2004).
7. T. Yasui, K. Sasaki, Y. Tohno, and T. Araki, "Tomographic imaging of collagen fiber orientation in human tissue using depth-resolved polarimetry of second-harmonic-generation light," Opt. Quantum Electron. **37**, 1397–1408 (2005).
8. A. K. Dunn, V. P. Wallace, M. Coleno, M. W. Berns, and B. J. Tromberg, "Influence of optical properties on two-photon fluorescence imaging in turbid samples," Appl. Opt. **39**, 1194–1201 (2000).
9. C.-Y. Dong, K. Koenig, and P. So, "Characterizing point spread functions of two-photon fluorescence microscopy in turbid medium," J. Biomed. Opt. **8**, 450–459 (2003).
10. U. K. Tirlapur, K. König, C. Peuckert, R. Krieg, and J. J. Halbhuber, "Femtosecond near infrared laser pulses elicit generation of reactive oxygen species in mammalian cells leading to apoptosis-like death," Exp. Cell Research **263**, 88–97 (2001).
11. K. König, P. T. C. So, W. W. Mantulin, and E. Gratton, "Cellular response to near-infrared femtosecond laser pulses in two photon microscope," Opt. Lett. **22**, 135–136 (1997).
12. P. C. Cheng, S. J. Pan, A. Shih, K.-S. Kim, W. S. Liou, and M. S. Park, "Highly efficient upconverters for multiphoton fluorescence microscopy," J. Microsc. **189**, 199–212 (1998).
13. R. R. Anderson and J. A. Parish, "The optics of human skin," J. Invest. Dermatol. **77**, 13–19 (1981).
14. S.-W. Chu, S.-Y. Chen, T.-H. Tsai, T.-M. Liu, C.-Y. Lin, H.-J. Tsai, and C.-K. Sun, "In vivo developmental biology study using noninvasive multi-harmonic generation microscopy," Opt. Express **11**, 3093–3099 (2003).
15. S.-P. Tai, W.-J. Lee, D.-B. Shieh, P.-C. Wu, H.-Y. Huang, C.-H. Yu, and C.-K. Sun, "In vivo optical biopsy of hamster oral cavity with epi-third-harmonic-generation microscopy," Opt. Express **14**, 6178–6187 (2006).
16. S.-P. Tai, T.-H. Tsai, W.-J. Lee, D.-B. Shieh, Y.-H. Liao, H.-Y. Huang, K. Zhang, H.-L. Liu, and C.-K. Sun, "Optical biopsy of fixed human skin with backward-collected optical harmonics signals," Opt. Express **13**, 8231–8242 (2005).
17. S.-Y. Chen, C.-Y. S. Hsu, and C.-K. Sun, "Epi-third and second harmonic generation microscopic imaging of abnormal enamel," Opt. Express **16**, 11670–11679 (2008).
18. I.-H. Chen, S.-W. Chu, C.-K. Sun, P.-C. Cheng, and B.-L. Lin, "Wavelength dependent damage in biological multi-photon confocal microscopy: a microspectroscopic comparison between femtosecond Ti:sapphire and Cr:forsterite laser sources," Opt. Quantum. Electron **34**, 1251–1266 (2002).
19. T.-H. Tsai, S.-P. Tai, W.-J. Lee, H.-Y. Huang, Y.-H. Liao, and C.-K. Sun, "Optical signal degradation study in fixed human skin using confocal microscopy and higher-harmonic optical microscopy," Opt. Express **14**, 749–758 (2006).
20. G. J. Tearney, M. E. Brezinski, J. F. Southern, B. E. Bouma, M. R. Hee, and J. G. Fujimoto, "Determination of the refractive index of highly scattering human tissue by optical coherence tomography," Opt. Lett. **20**, 2258–2260 (1995).
21. L. Sherman, J. Y. Ye, O. Albert, and T. B. Norris, "Adaptive correction of depth-induced aberrations in multiphoton scanning microscopy using a deformable mirror," J. Microsc. **206**, 65–71 (2002).
22. P. Marsh, D. Burns, and J. Girkin, "Practical implementation of adaptive optics in multiphoton microscopy," Opt. Express **11**, 1123–1130 (2003).
23. Y. Jiang, I. Tomov, Y. Wang, and Z. Chen, "Second-harmonic optical coherence tomography," Opt. Lett. **29**, 1090–1092 (2004).
24. J. Su, I. V. Tomov, Y. Jiang, and Z. Chen, "High-resolution frequency-domain second-harmonic optical coherence tomography," Appl. Opt. **46**, 1770–1775 (2007).
25. Y. Guo, P. P. Ho, H. Savage, D. Harris, P. Sacks, S. Schantz, F. Liu, N. Zhadin, and R. R. Alfano, "Second-harmonic tomography of tissues," Opt. Lett. **22**, 1323–1325 (1997).
26. F. Fischer, B. Volkmer, S. Puschmann, R. Greinert, W. Breitbart, J. Kiefer, and R. Wepf, "Risk estimation of skin damage due to ultrashort pulsed, focused near-infrared laser irradiation at 800 nm," J. Biomed. Opt. **13**, 041320 (2008).
27. S.-Y. Chen and C.-K. Sun, "In vivo imaging of human skin using harmonic generation microscopy," in *Abstracts. Focus on Microscopy 2008* (2008), p. 59.
28. L. H. Kligman, E. Schwartz, A. N. Sapadin, and A. M. Kligman, "Collagen loss in photoaged human skin is overestimated by histochemistry," Photodermatol. Photoimmunol. Photomed. **16**, 224–228 (2000).
29. S.-J. Lin, R.-Jr. Wu, H.-Y. Tan, W. Lo, W.-C. Lin, T.-H. Young, C.-J. Hsu, J.-S. Chen, S.-H. Jee, and C.-Y. Dong, "Evaluating cutaneous photoaging by use of multiphoton fluorescence and second-harmonic generation microscopy," Opt. Lett. **30**, 2275–2277 (2005).
30. M. J. Koehler, K. König, P. Elsner, R. Bückle, and M. Kaatz, "In vivo assessment of human skin aging by multiphoton laser scanning tomography," Opt. Lett. **31**, 2879–2881 (2006).
31. T. Yasui, Y. Takahashi, T. Araki, Y. Ogura, Y. Matsunaga, and T. Kuwahara, "Observation of photoaged, dermal collagen fiber using polarization-resolved second-harmonic-generation microscopy," J. Invest. Dermatol. **128**, S40 (2008).
32. T. Yasui, Y. Takahashi, S. Fukushima, Y. Ogura, T. Yamashita, T. Kuwahara, T. Hirao, and T. Araki, "Observation of dermal collagen fiber in wrinkled skin using polarization-resolved second-harmonic-generation microscopy," Opt. Express **17**, 912–923 (2009).1234